

Predictions for the diffuse cosmic dipole at radio frequencies from reionization imprints

T. Trombetti^{1,*} and C. Burigana^{1,2,3}

¹ INAF, Istituto di Radioastronomia, Via Piero Gobetti 101, I-40129 Bologna, Italy

² Dipartimento di Fisica e Scienze della Terra, Università di Ferrara, Via Giuseppe Saragat 1, I-44122 Ferrara, Italy

³ INFN, Sezione di Bologna, Via Irnerio 46, I-40127 Bologna, Italy

Received ...; accepted ...

ABSTRACT

The cosmological reionization and thermal history, following the recombination epoch and the dark age, can be studied at radio frequencies through the tomographic view offered by the redshifted 21-cm line and the integrated information carried out by the diffuse free-free emission, coupled to the Comptonization distortion, which is relevant at higher frequencies. For the both types of signals, current theoretical predictions span a wide range of possibilities, while the recent EDGES observations of the monopole disagree with the typical standard models and call, if confirmed, for non-standard physical processes and/or for an early population of extragalactic sources producing a remarkable radio background at high redshifts almost consistent with the ARCADE 2 claim of a significant excess of CMB absolute temperature at low frequency. These signatures can be observed both in global (or monopole) signal and fluctuations, from very large to small angular scales. The peculiar motion of an observer with respect to an ideal reference frame in rest with respect to the CMB produces boosting effects in several observable quantities, that are remarkable in the anisotropy patterns at low multipoles, and in particular in the dipole, with frequency spectral behaviours depending on the spectrum of the monopole emission, as already studied in the context of CMB spectral distortions. We present here a novel investigation of this effect at radio frequencies, aimed at predicting the imprints expected in the redshifted 21-cm line signal and in the diffuse free-free emission plus the Comptonization distortion for several representative models. Furthermore, we consider the same type of signal but expected from the cosmological (CMB plus potential astrophysical signals) radio background determining the offset for 21-cm redshifted line. The combination of the four types of signal and their different relevance in the various frequency ranges is studied. This approach, linking monopole and anisotropy analyses, can be applied on all-sky or relatively wide sky coverage surveys as well as to a suitable set of sky patches, and, relying only on the quality of interfrequency and relative data calibration, in principle by-pass the need for precise absolute calibration, a critical point of current and future radio interferometric facilities.

Key words. Diffuse radiation; cosmic background radiation; dark ages, reionization, first stars.

1. Introduction

The recent results from the *Planck* satellite support cosmological reionization scenarios almost compatible with astrophysical models for the evolution of structure, galaxy and star formation. On the other hand, the full understanding of the reionization and thermal history of the Universe since recombination epoch is still far to be consolidated and it is important to discriminate among the various models compatible with current data. The radio to sub-millimetre background provides a very important window for studying this process in a global approach and achieving a complete comprehension of the involved photon and energy sources. We mainly focus here on the information carried out at radio frequencies, where the redshifted 21-cm line from neutral hydrogen offers a tomographic view of the process and the diffuse free-free (FF) emission provides a fundamental information integrated over the relevant epochs. Furthermore, the precise understanding of the radio extragalactic background is linked to the comprehension of these signals.

The peculiar motion of an observer with respect to an ideal reference frame, in rest with respect to the cosmic microwave background (CMB), produces boosting effects in the anisotropy patterns at low multipoles, in particular in the dipole, with fre-

quency spectral behaviour related to the spectrum of the corresponding monopole emission. The possibility of studying the dipole anisotropy spectrum to extract information on the CMB spectral distortions has been originally proposed (Danese & de Zotti 1981) with the aim of constraining energy dissipations possibly occurred in the cosmic plasma at different epochs, focussing on Bose-Einstein like and Comptonization distortions. This topic has been recently investigated in the context of future CMB anisotropy missions (Balashev et al. 2015), including also the possibility of better constraining the cosmic infrared background (CIB) spectrum (De Zotti et al. 2016), and considering both these topics including instrumental performance as well as limitations by foregrounds and relative calibration uncertainties, also through numerical simulations (Burigana et al. 2018). The possibility of applying this differential approach to the analysis of the redshifted 21-cm line has been advanced by Slosar (2017), while Deshpande (2018) proposed to exploit the corresponding diurnal pattern in drift-scan observations.

In this work we present the predictions for the diffuse cosmic dipole, mainly at radio frequencies but in some cases also in the microwave/sub-millimetre domain, from four types of imprints and their combinations expected from (or associated to) cosmological reionization, namely the diffuse FF emission and the coupled Comptonization distortion, the redshifted 21-cm line

* e-mail: trombetti@ira.inaf.it

and the radio extragalactic background, for a set of models spanning currently plausible ranges of possibilities.

In Sect. 2 we present and discuss the models adopted for the monopole spectra, including different extragalactic residual radio backgrounds from source contribution subtractions at different detection thresholds. In Sect. 3 we briefly describe the adopted differential approach basic formalism. Our main results for each specific type of signal are presented in Sect. 4, while those regarding the dipole spectra expected from combinations of these imprints are described in Sect. 5. Finally, in Sect. 6 we draw our main conclusions.

2. Monopole models

2.1. Joint free-free diffuse emission and Comptonization distortion

The cosmological reionization process associated with the primeval formation phases of bound structures, sources of photon and energy production, generates coupled Comptonization distortions, because of electron heating (Zel'dovich et al. 1972), and FF distortions. The key parameters for characterizing these effects as functions of time are the Comptonization parameter

$$u(t) = \int_{t_i}^t [(\phi - \phi_i)/\phi](kT_e/mc^2)n_e\sigma_T c dt \quad (1)$$

and the FF distortion parameter $y_B(t, x)$

$$\begin{aligned} y_B(t, x) &= \int_{t_h}^t (\phi - \phi_i)\phi^{-3/2} g_B(x, \phi) K_{0B} dt \\ &= \int_z^{z_h} (\phi - \phi_i)\phi^{-3/2} g_B(x, \phi) K_{0B} t_{exp} \frac{dz}{1+z}, \end{aligned} \quad (2)$$

where z is the redshift, T_e the electron temperature, t_{exp} the cosmic expansion time and $K_{0B}(z) = K_B(z)/\phi^{-7/2}$, being $K_B(z)$ expressed by

$$\begin{aligned} K_B(z) &= \frac{8\pi}{3} \frac{e^6 h^2 n_e (n_H + 4n_{He})}{m(6\pi m k T_e)^{1/2} (k T_e)^3} \\ &\sim 2.6 \cdot 10^{-25} \phi^{-7/2} (T_0/2.7K)^{-7/2} (1+z)^{5/2} \hat{\Omega}_b^2 \chi_e^2 \text{ sec}^{-1}. \end{aligned} \quad (3)$$

In the above equations $x = h\nu/(kT_r)$ and $T_r = T_0(1+z)$ are the redshift invariant dimensionless frequency and the redshift dependent CMB effective temperature, $g_B(x, \phi)$ is the Gaunt factor, $\phi = T_e/T_r$ and $\hat{\Omega}_b = \Omega_b h_{50}^2$, with $h_{50} = H_0/(50 \text{ km sec}^{-1} \text{ Mpc}^{-1})$, H_0 the Hubble constant and Ω_b the baryon density parameter. Here, $T_0 = (2.72548 \pm 0.00057) \text{ K}$ (Fixsen 2009) is the current CMB effective temperature in the blackbody spectrum approximation, i.e. such that aT_0^4 gives the present CMB energy density. In Eqs. (1) and (3), n_e is the density of free electrons, a mixture of hydrogen and helium with densities in the ionized state n_H and n_{He} is assumed for simplicity in the first equality of Eq. (3), while the approximation in the second equality of Eq. (3) explicates the dependence on the ionization degree, χ_e .¹ In the above equations, k and h are the Boltzmann and Planck constant, m is the electron mass, c the speed of light, σ_T the Thomson cross section and $\phi_i = \phi(z_i) = (1 + \Delta\epsilon/\epsilon_i)^{-1/4} \simeq 1 - u$ is the ratio between the equilibrium matter temperature and the radiation temperature at the beginning of the heating process (i.e., at z_i).

¹ A more accurate formula, according to the convention adopted to define χ_e , should include the atom fractions in different ionization states (see, e.g., Trombetti & Burigana (2014)), but this is not relevant in the context of this paper.

The distorted photon occupation number is well approximated by

$$\eta^{\text{FF+C}} \simeq \eta_i + u \frac{x/\phi_i \exp(x/\phi_i)}{[\exp(x/\phi_i) - 1]^2} \left(\frac{x/\phi_i}{\tanh(x/2\phi_i)} - 4 \right) + \frac{y_B(x)}{x^3} \quad (4)$$

where η_i is the initial photon occupation number (i.e. before the beginning of the dissipation process). In the following, η_i will be assumed to have a Planckian distribution. At low frequencies $\eta^{\text{FF+C}}$ can be approximated by the expression:

$$\eta^{\text{FF+C}} \simeq \eta_i + \frac{y_B(x)}{x^3} - \frac{2u}{x/\phi_i} \simeq \frac{1-3u}{x} + \frac{y_B(x)}{x^3}. \quad (5)$$

Eqs. (1), (2) and (4) hold at any redshift, provided that the two distortion parameters, y_B and u , are integrated over the corresponding redshift interval. Performing the integral over the relevant cosmic times and in the limit of small energy injections (accordingly to current limits), one gets the relation between u and the global fractional energy exchange between matter and radiation in the cosmic plasma: $u \simeq (1/4)\Delta\epsilon/\epsilon_i$.

Defining the thermodynamic temperature, $T_{th}(\nu)$, as the temperature of the blackbody having the same $\eta(\nu)$ at the frequency ν ,

$$T_{th}(\nu) = \frac{h\nu}{k} \frac{1}{\ln(1 + 1/\eta(\nu))}, \quad (6)$$

the CMB spectrum can be approximated at low frequencies by the relation

$$T_{th}^{\text{FF+C}}(x) \simeq \left(\frac{y_B(x)}{x^2} - 2u\phi_i + \phi_i \right) T_r, \quad (7)$$

and

$$\frac{\Delta T_{exc}^{\text{FF}}}{T_r} \simeq \frac{y_B(x)}{x^2} \quad (8)$$

quantifies the relative excess over T_r due to the FF diffuse emission.

In the above equations a uniform medium is assumed. This is not critical for the global Comptonization distortion, since it depends linearly on matter density, but it introduces a significant underestimation of the FF distortion in the presence of substantial intergalactic medium (IGM) matter density contrast, because of bremsstrahlung quadratic dependence on matter density.

A separation approach, resulting in agreement with numerical simulations (Ponente et al. 2011), has been adopted to take into account inhomogeneities in matter density (Trombetti & Burigana 2014).² It allows a versatile modeling of thermal and ionization histories for different underlying cosmological models. Defining the density as the sum of a mean term and a small perturbation and averaging over a volume representative of the Universe, a time dependent clumping factor, $(1 + \sigma^2)$, accounts for inhomogeneities in the bremsstrahlung rate, by replacing $\Omega_b^2(z) = \Omega_{b,homog}^2 (1 + \sigma^2(z))$, where $\Omega_{b,homog}^2$ defines the homogeneous case. The baryonic matter variance, $\sigma^2(z)$, is influenced by the dark matter (DM) particles nature especially at high wavenumbers \tilde{k} , while large scale structure distribution is almost independent of the model (Gao & Theuns 2007). The intrinsic

² In principle, higher order corrections from inhomogeneities in the medium temperature, as well as differences in the inhomogeneities of free electrons and atoms in different ionization states, could also be included. On the other hand, these terms are expected to be significantly smaller than the leading correction considered here.

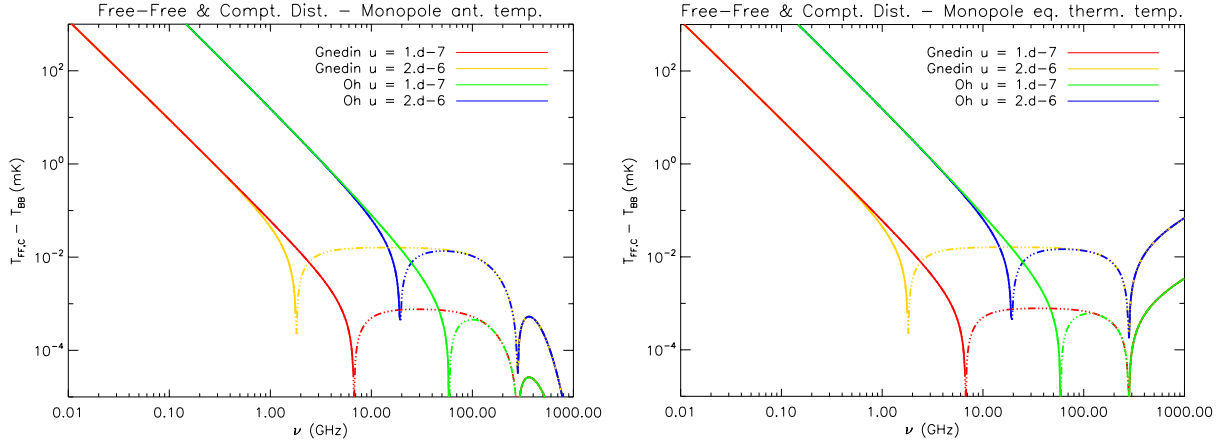


Fig. 1. Monopole signal for the considered combined Comptonization and diffuse FF distortion models after subtraction of the current CMB spectrum in the blackbody approximation at the effective temperature T_0 . Solid and three dots-dashed lines refer to positive and negative values, respectively. Free-free distortions are evaluated for a reionization model compatible with *Planck* results and for an extreme model involving a population of ionized halos. Comptonization distortions are evaluated for $u = 2 \times 10^{-6}$ and $u = 10^{-7}$, representative of imprints by astrophysical or minimal reionization models. For comparison with previous works focussed on CMB, they are displayed, other than in terms of antenna temperature (left panel) typically used at radio frequencies, also in terms of equivalent thermodynamic temperature (right panel), the differences appearing above ≈ 40 GHz. See also the legend and the text.

thermal velocities of warm DM particles imply a suppression of small scale structures formation, efficient below their free-streaming scale, with a delay of the growth of structures (Viel et al. 2005). This loss of power in warm DM models can be approximated by a cold DM model with a suitable cut-off, k_{max} , in the typical range $\approx (20 \div 10^3)$, according to particle thermal properties. Thus, $\sigma^2(z)$ mainly depends on two crucial parameters, the amplitude and the cut-off of perturbations.

As examples, we consider two pairs of different FF and Comptonization distortion models. We first adopt the FF model described in Trombetti & Burigana (2014) for the ionization history of Gnedin (2000), resulting into a Thomson optical depth τ well consistent with recent *Planck* results, and a fixed cut-off value $k_{max} = 100$. We couple it with two different levels of Comptonization distortion, characterized by $u = 10^{-7}$, very close to that derived in Burigana et al. (2008) for the Gnedin (2000) model and corresponding to an almost minimal energy injection consistent with the current constraints on τ , and by $u = 2 \times 10^{-6}$, a value accounting for possible extra energy injections by a broad set of astrophysical phenomena. While larger FF distortions (up to a factor of about 1.5–2) derive from larger values of k_{max} or from ionization histories with slightly larger values of τ , the FF diffuse emission from an ensemble of ionized halos at substantial redshifts is expected to generate much larger signals. Remarkably, the model by Oh (1999) predicts a very large global (i.e. integrated over the ensemble of halos) FF signal, corresponding to $y_B \sim 1.5 \times 10^{-6}$ at $\nu \sim 2$ GHz.³ Thus, we rescale the above FF model to $y_B(2 \text{ GHz}) = 1.5 \times 10^{-6}$, coupled with Comptonization distortions with $u = 10^{-7}$ or 2×10^{-6} . These four models likely identify a plausible range of possible distortions.⁴ They

are shown in Fig. 1, after the subtraction of the current CMB spectrum in the blackbody approximation at its effective temperature, both in terms equivalent thermodynamic temperature (right panel) and antenna temperature (left panel)

$$T_{ant}(\nu) = \frac{h\nu}{k} \eta(\nu). \quad (9)$$

Note the change from positive to negative values, predicted at a frequency ranging from a few GHz to several tens of GHz, according to the amplitude of FF emission and the value of u . Almost independently of the - Comptonization - distortion level, a well known change from negative to positive values occurs at ≈ 280 GHz.⁵

At extremely low frequencies, Eq. (4) should be replaced by a more accurate formula (see, e.g., eq. (33) in Burigana et al. (1995)) for the bremsstrahlung process, since the extremely high efficiency of the process implies the achievement of a blackbody spectrum at electron temperature. On the other hand, the simple representation in terms of y_B expressed by Eqs. (4) and (7), predicting a continuous equivalent thermodynamic temperature increase at decreasing frequency, well approximates the exact solution in the observable frequency range (see Appendix A).

At low frequencies, y_B can be approximated by a power law

$$y_B(\nu) \simeq A_{FF} (\nu/\text{GHz})^{-\zeta} \quad (10)$$

with $\zeta \approx 0.15$, and $A_{FF} \approx 7.012 \times 10^{-9}$ or 1.664×10^{-6} for the two considered models.

Explorer (COBE), and on y_B derived including also previous low frequency measurements (Salvaterra & Burigana 2002) and the TRIS data (Gervasi et al. 2008b), that sets $-6.3 \times 10^{-6} < y_B < 12.6 \times 10^{-6}$ (at 95% CL), and, obviously, within the relaxation of y_B limits, $|y_B| < 10^{-4}$ (Seiffert et al. 2011), mainly due to the excess (Singal et al. 2011) at ≈ 3.3 GHz in the second generation of the Absolute Radiometer for Cosmology, Astrophysics, and Diffuse Emission (ARCADE 2) data (if not explained by a population of faint radio sources; see also Sect. 2.3).

⁵ Note that, for global distortions and referring to the current - i.e. after heating - directly observable CMB effective temperature T_0 , this change of sign occurs at a frequency slightly higher than ≈ 220 GHz that holds for the thermal Sunyaev-Zel'dovich effect on a galaxy cluster.

³ This level of global FF diffuse emission was found by Oh (1999) integrating the number counts of FF emitters over the whole astrophysical range, i.e. without any subtraction of signals by individual ionized halos. Applying a subtraction of FF emitters down to faint detection thresholds, as feasible with high resolution and deep surveys as, e.g., SKA, the residual FF diffuse emission will be significantly lower.

⁴ The studied range for Comptonization and FF distortions are well within the current observational constraints on u , $|u| \leq 1.5 \times 10^{-5}$ (at 95% CL), mainly coming from the Far Infrared Absolute Spectrophotometer (FIRAS) (Fixsen et al. 1996) on board the Cosmic Background

2.2. 21-cm redshifted line

A precise measure and mapping of the redshifted 21-cm line signal with current and next-generation of radio telescopes is likely the best way to investigate on the evolution and distribution of neutral Hydrogen (*HI*) in the Universe from the Dark Ages to the reionization history (Epoch of Reionization, EoR).

This 21-cm line corresponds to the spin-flip transition in the ground state of neutral hydrogen. In cosmology, the 21-cm signal, usually expressed in terms of antenna temperature, is described as the offset of the 21-cm brightness temperature from the CMB temperature, T_{CMB} , along the observed line of sight at frequency ν and is given by (Furlanetto et al. 2006):

$$T_{\text{ant}}^{21\text{cm}}(\nu) = \frac{T_S - T_{\text{CMB}}}{1+z} (1 - e^{-\tau_{\nu_0}}) \\ \approx 27x_{\text{HI}} \left(1 - \frac{T_{\text{CMB}}}{T_S}\right) (1 + \delta_{\text{nl}}) \left(\frac{H(z)}{dv_r/dr + H(z)}\right) \\ \sqrt{\frac{1+z}{10} \frac{0.15}{\Omega_m h_{100}^2} \left(\frac{\Omega_b h_{100}^2}{0.023}\right)} \text{mk}, \quad (11)$$

where T_S is the gas spin temperature, which represents the excitation temperature of the 21-cm transition, x_{HI} is the neutral hydrogen fraction, τ_{ν_0} is the optical depth at the 21-cm frequency ν_0 , $H(z)$ is the Hubble function, Ω_m is the (non-relativistic) matter density parameter, $h_{100} = H_0/(100 \text{ km s}^{-1} \text{ Mpc}^{-1})$, $\delta_{\text{nl}}(\mathbf{x}, z) \equiv \rho/\bar{\rho} - 1$ is the evolved (Eulerian) density contrast, dv_r/dr is the comoving gradient of the line of sight component of the comoving velocity, and all the terms are computed at redshift $z = \nu_0/\nu - 1$. The CMB is assumed as a backlight, thus if $T_S < T_{\text{CMB}}$ the gas is seen in absorption, while if $T_S > T_{\text{CMB}}$ it appears in emission. More in general, T_{CMB} should include not only the CMB (blackbody) background defined by T_r but also potential distortions and other possible radiation backgrounds relevant at radio frequencies. Eq. (11) shows a dependence on both the IGM temperature and ionization evolution, as well as fundamental cosmological parameters.

Since the 21-cm signal is a line transition, its frequency redshifts from each specific cosmic time during the EoR up to the current time into a well defined frequency. The signal detected at a given frequency, then, refers to a particular redshift, implying that the 21-cm analysis constitutes a unique tomographic observation of cosmic evolution.

Different models predict different gas ionization fraction and spin temperature evolutions and, correspondingly, different predictions for the global 21-cm background signal, $T_{\text{ant}}^{21\text{cm}}(\nu)$, related to the underlying astrophysical emission sources and feedback mechanisms. A wide set of models have been considered in Cohen et al. (2017), resulting into an envelope of possible predictions for $T_{\text{ant}}^{21\text{cm}}(\nu)$.

Recent limits on the global 21-cm background signals have been set by Bernardi et al. (2016) applying to a 19-min-long observation from the Large aperture Experiment to detect the Dark Ages (LEDA) a fully Bayesian method to identify the faint signal from the much brighter foreground emission. They found a signal amplitude between -890 and 0 mK (at 95% CL) in the frequency range $100 > \nu > 50$ MHz corresponding to a redshift range $13.2 < z < 27.4$. These data set limits on the 21-cm signal from the cosmic dawn before or at the beginning of the electron ionization fraction increase, constraining structures and IGM thermal history in connection with heating sources.

Surprisingly, a pronounced absorption profile, with an almost symmetric U-shape, centred at (78 ± 1) MHz has been recently

found by Bowman et al. (2018) analysing a set of observational campaigns, started in August 2015, carried out with low-band instruments of the Experiment to Detect the Global Epoch of Reionization Signature (EDGES). The amplitude of the absorption feature is found to be of $0.5^{+0.5}_{-0.2}$ K, more than a factor of two greater than those predicted by the most extreme astrophysical models (Cohen et al. 2017) that unlikely account for a such deep signature. The spread of the profile has a full-width at half-maximum of 19^{+4}_{-2} MHz, the low-frequency edge supporting the existence of a ionizing background by 180 million years after the Big Bang, the high-frequency edge indicating that the gas was heated to above the radiation temperature less than 100 million years later (Bowman et al. 2018).

We consider six models (displayed in Fig. 2), the first being the analytical representation of EDGES absorption profile, the other five falling in the region of the $\nu - T_{\text{ant}}^{21\text{cm}}$ plane identified in Cohen et al. (2017). One model is presented in Schneider et al. (2008) for the ionization history of Gnedin (2000), already considered for the FF diffuse emission in the Sect. 2.1, another is the standard case model in Cohen et al. (2017). Other three models, taken into account also in the study for the Square Kilometre Array (SKA) by Subrahmanyan et al. (2015) and labelled SKA, SKA1 and SKA2, come from Pritchard & Loeb (2010), exploiting the dependence of 21-cm signal on the X-ray emissivity ($f_X = 0.01$ and $f_X = 1$), and from Burns et al. (2012) (case of no heating model). Fig. 2 shows that the spectral shapes predicted for the redshifted 21-cm line global signal present substantial differences from one model to another, differently from the combined Comptonization and FF distortion that, at least to a good approximation, simply rescales according to two global parameters. The six models considered here, far from representing the full set of possibilities, span a wide range of behaviors and amplitudes. They will be exploited in next sections to illustrate the expected types of diffuse dipole signal. Note also that they are predicted to be relevant in a limited range of frequencies. In that range, the amplitudes of the combined FF diffuse emission and of the redshifted 21-cm line global signal span over a similar and model dependent range, but their spectral shapes are very different.

2.3. Extragalactic background

The signals discussed in Sects. 2.1 and 2.2, tightly related to the ionization and thermal history of IGM, although coupled with clumping and galaxy evolution, are intrinsically diffuse. An important extragalactic background signal is expected from the integrated contribution of discrete sources. A large fraction of it can be resolved through galactic surveys going down and down in flux density level. In spite of this, a residual background, observationally diffuse, comes from the contribution of faint sources below survey detection limits, and depends on their number counts. This signal is, in general, very high compared to the fine signatures directly coming from reionization. Other than intrinsically interesting, this extragalactic background needs to be accurately known in order to faithfully understand the reionization imprints. Remarkably, these classes of signals may be also tightly related. Indeed, as shown in Eq. (11), the explanation of the 21-cm redshifted line signal found by EDGES could require, other than a substantial cooling of the IGM gas, at a temperature well below that of the standard adiabatic prediction, driven by interactions between DM and baryons (Barkana 2018; Muñoz & Loeb 2018), an additional high redshift extragalactic radio background, much larger than the CMB one for a blackbody spectrum at an equilibrium temperature equal to the one

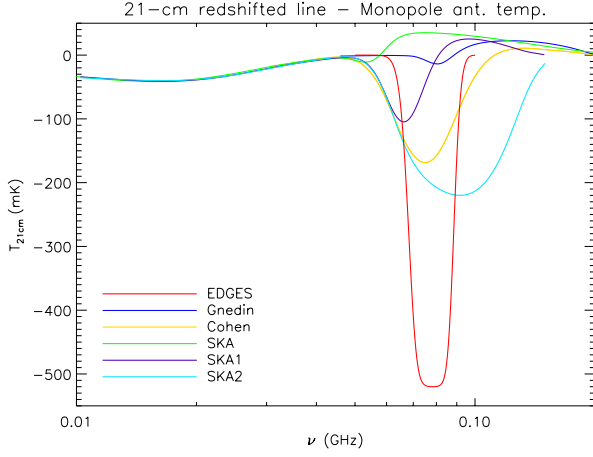


Fig. 2. Monopole signal in terms of antenna temperature for the considered models of redshifted 21-cm line. Note that the deepness of the EDGES profile is greater by a factor of ≈ 3 than that of the standard case model in Cohen et al. (2017). Different models predict signals with sign changes or vanishing values at different frequencies. Since the effect is important at low frequencies, antenna and equivalent thermodynamic temperatures are typically similar, but not for small values of T_{ant} (below some tens of mK) and particularly when it vanishes or tends to vanish. See also the legend and the text.

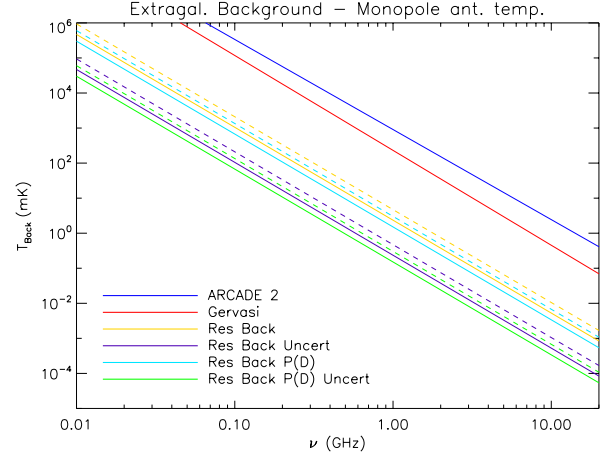


Fig. 3. Monopole signal in terms of antenna temperature for the two considered extragalactic background models and various estimates of extragalactic source background signal for different assumptions of source contribution subtraction. The labels "Res Back" and "Res Back P(D)" refer, respectively, to the choice of $A = 2.35$ and 1.51 mK in Eq. 14, while the additional label "Uncert" includes a reduction by factor of 10; dashed lines refer to the same estimates, but derived assuming an increasing of a factor of 2 in the differential number counts at faint flux densities. See also the legend and the text.

observed by FIRAS and rescaled by $1 + z$. A first claim of a notable extragalactic radio background⁶ was proposed by Seiffert et al. (2011) to explain the signal excess found by ARCADE 2, whose spectral shape was too steep to be well accounted by a fit in terms of FF emission. In principle, this excess could be an intrinsic CMB feature or could be ascribed to a substantial astrophysical contribution generated, e.g., by a faint population of radio sources (Feng & Holder 2018), or by a strong emission, with heavy obscuration or a large radio loud fraction, associated to black holes / Pop-III stars evolution at $z \gtrsim 17$ and with a growth declining at $z < 16$ (Ewall-Wice et al. 2018), or by black hole high mass X-ray binary microquasars (Mirabel 2019). Note that, according to Seiffert et al. (2011), the limits on FF distortion significantly change assuming or not the presence of a substantial extragalactic source radio background.

We exploit several simple analytical representations of the extragalactic radio background. Some of them will be adopted in next sections to illustrate the expected types of dipole signal.

Initially, we assume the power law best fit model

$$T_{\text{ant}}^{\text{Back}}(\nu) \simeq 18.4 \text{ K} (\nu/0.31 \text{ GHz})^{-2.57} \quad (12)$$

by Seiffert et al. (2011) (expressed in terms of antenna temperature).

A careful analysis and prediction of the extragalactic source radio background, also including different source detection thresholds, has been carried out by Gervasi et al. (2008a). We consider their single power law best fit model for the extragalactic source background signal (again in terms of antenna temperature)

$$T_{\text{ant}}^{\text{Back}}(\nu) \simeq 0.88 \text{ K} (\nu/0.61 \text{ GHz})^{-2.707} \quad (13)$$

The authors provided an empirical analytical fit function of the differential number counts normalized to the Euclidean distribution of sources. With this recipe, we estimated the extragalactic radio background proportional to $\int_{S_{\text{min}}}^{S_{\text{max}}} S N'(\nu) dS$, where $N'(\nu)$

⁶ See also the recent radio data by Dowell & Taylor (2018).

are the differential number counts.⁷ Since the authors found a reasonable convergence of the integration extending S_{min} down to 10^{-12} Jy, the extragalactic radio background can be computed assuming S_{max} as single parameter, to be set according to the considered source detection threshold. We fit the results computed in the frequency range between 0.151 GHz and 8.44 GHz investigated by the authors for certain values of S_{max} . We find that a simple power law represents a good approximation, given the current uncertainties on number counts at faint flux densities. As examples of numerical estimates, we assume $S_{\text{max}} = 50$ nJy, almost corresponding to typical detection limits of the Ultra Deep reference continuum surveys planned for SKA (Prandoni & Seymour 2015), and $S_{\text{max}} = 15$ nJy, since number counts down to flux densities fainter than detection threshold can be investigated through $P(D)$ methods (see Vernstrom et al. (2014) for an analysis at 3 GHz; see also Vernstrom et al. (2016)). Fitting the results for the extragalactic radio background up to these flux densities we find

$$T_{\text{ant}}^{\text{Back}}(\nu) \simeq A (\nu/\text{GHz})^{-2.65} \quad (14)$$

with, respectively, $A \simeq 2.35$ and 1.51 mK. The authors found also an uncertainty from $\approx 6\%$ to $\approx 30\%$ from lowest to highest frequencies in the above estimate. Taking a $\approx 10\%$ uncertainty at all frequencies in this characterization, the remaining residual extragalactic radio background is found to be smaller by a factor ≈ 10 with respect to the above estimate.

The discussed models are shown in Fig. 3 (solid lines). Obviously, a deeper source subtraction and a better modeling imply a lower effective extragalactic radio background to be taken into account.

Recently, the Lockman Hole Project and deep Low Frequency Array (LOFAR) imaging of the Boötes field have indicated a certain flattening of differential number counts at 1.4 GHz below $\approx 100 \mu\text{Jy}$ (Prandoni et al. 2018) and at 0.15 GHz below ≈ 1 mJy (Retana-Montenegro et al. 2018), respectively,

⁷ When a range for the parameters of the fit representation of $N'(\nu)$ is provided, we assume, for simplicity, their central values.

suggesting an increasing of differential number counts of a factor of ~ 2 with respect to the estimate of Gervasi et al. (2008a) at the faint flux densities adopted above for computing the integral of $SN'(\nu)dS$, likely related to the emerging of star forming galaxies and radio-quiet AGNs at fainter flux densities. This directly translates into an extragalactic radio background estimate a factor of ~ 2 larger, displayed with dashed lines in Fig. 3.

3. Differential approach basic formalism

The peculiar motion of an observer with respect to an ideal reference frame, set in rest with respect to the CMB, produces boosting effects in several observable quantities, the largest of which is the dipole, i.e. the multipole $\ell = 1$ anisotropy in the Solar System barycentre frame.

The peculiar velocity effect on the frequency spectrum can be evaluated on the whole sky using the complete description of the Compton-Getting effect (Forman 1970). It is based on the Lorentz-invariance of the photon distribution function. At a given ν , the photon distribution function, $\eta^{\text{BB/dist}}$, should be computed, for the considered type of spectrum, with the frequency multiplied by the product $(1 - \hat{n} \cdot \beta)/(1 - \beta^2)^{1/2}$ that accounts for all the possible sky directions with respect to the observer peculiar velocity, defined by the unit vector \hat{n} and the vector β . So, all the orders in β and the link with the geometrical properties induced at each multipole are included. The notation ‘BB/dist’ stands for a blackbody spectrum or for any type of non pure blackbody signal, namely, the FF plus Comptonization (C) distortion or the 21-cm redshifted line global signal, for reionization imprints, or the extragalactic radio background, or combinations of them. In terms of equivalent thermodynamic temperature the observed signal map is given by (Burigana et al. 2018):

$$T_{\text{th}}^{\text{BB/dist}}(\nu, \hat{n}, \beta) = \frac{xT_0}{\ln(1/(\eta(\nu, \hat{n}, \beta))^{\text{BB/dist}} + 1)}; \quad (15)$$

here $\eta(\nu, \hat{n}, \beta) = \eta(\nu')$ with $\nu' = \nu(1 - \hat{n} \cdot \beta)/(1 - \beta^2)^{1/2}$.

Eq. (15) generalizes the result found by Danese & de Zotti (1981) for the difference in T_{th} measured in the direction of motion and in its perpendicular direction, expressed by

$$\Delta T_{\text{th}} = \frac{h\nu}{k} \left\{ \frac{1}{\ln[1 + 1/\eta(\nu)]} - \frac{1}{\ln[1 + 1/\eta(\nu(1 + \beta))]} \right\}, \quad (16)$$

whose first order approximation, given by

$$\Delta T_{\text{th}} \simeq - \frac{x\beta T_0}{(1 + \eta) \ln^2(1 + 1/\eta)} \frac{d \ln \eta}{d \ln x}, \quad (17)$$

underlines the contribution to the spectrum of the dipole, coming from the first logarithmic derivative of the photon occupation number with respect to the frequency. Different spectral shapes of monopole signals under consideration will translate into different dipole spectra.

In the next sections we will compute the effect at radio frequencies through the Eq. (16)⁸ for the various monopole signals described in Sect. 2. For numerical estimates, we will assume the CMB dipole to be due to velocity effects only and set $\beta = A_{\text{dip}}/T_0 = 1.2345 \times 10^{-3}$, being $A_{\text{dip}} = (3.3645 \pm 0.002) \text{ mK}$

⁸ Note that, in principle, the difference in T_{th} expressed by Eq. (16) includes also the contributions from multipoles $\ell > 1$. Anyway, they introduce (small) higher order corrections (see, e.g., the quadrupole and octupole maps computed in Burigana et al. (2018)) neglected in this work in numerical computations.

the nominal CMB dipole amplitude as from *Planck* 2015 results (Planck Collaboration 2016a,b,c).⁹

4. Single signal results

In this section we present the dipole spectra behaviours derived for the signal discussed.

Fig. 4 illustrates the dipole spectra for the combination of FF and Comptonization distortion. In the plot, we subtract the “reference” dipole spectrum corresponding to the blackbody at the current temperature T_0 . The (positive) FF term dominates at low frequencies, the (negative) Comptonization term at high frequencies. The transition from the FF to the Comptonization regime, ranging from about 3 GHz to about 100 GHz, depends on the relative amplitude of the two parameters y_B and u . These frequencies are of potential interest both for the CMB missions extending in frequency below the minimum of foreground contamination, and for radio surveys. Note the agreement at high frequencies with the results found in Burigana et al. (2018) (see their figure 7) where FF emission was neglected. For $u \sim 10^{-7}$ (respectively $u \sim 2 \times 10^{-6}$) the FF term dominates at frequencies below about 10 GHz to 100 GHz (respectively 3 GHz to 30 GHz) going from almost minimal to extreme FF models.

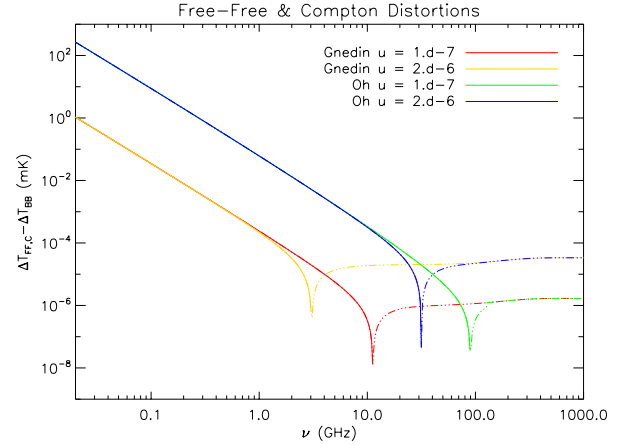


Fig. 4. Spectrum of dipole (in equivalent thermodynamic, or CMB, temperature) expressed as the difference between that produced in the presence of a FF distortion (dominant at low frequencies) plus a Comptonization distortion (dominant at high frequencies) with monopole spectra as in Fig. 1 and that corresponding to the blackbody at the current temperature T_0 . Thick solid lines (or three dots-dashes) correspond to positive (or negative) values. See also the legend and the text.

Fig. 5 shows the 21-cm redshifted line dipole spectra, where we first add (in η) its contribution with the one from the CMB blackbody at the current temperature T_0 , compute the resulting dipole¹⁰ and then, as before, subtract the dipole spectrum for the reference blackbody case.

For each model, note how the monopole signal behaviour changes are reflected into the sign inversions in the dipole spectrum (see Eq. (17)). Clearly, a larger monopole amplitude and shape steepness typically imply a larger dipole amplitude. Their combined effect is remarkable for the EDGES profile, its dipole

⁹ While the *Planck* 2018 result by the LFI (Planck Collaboration et al. 2018c) is almost identical to the nominal *Planck* 2015 result, the HFI one (Planck Collaboration et al. 2018b) indicates a slightly lower value, $A_{\text{dip}} = 3.36208 \text{ mK}$, still compatible within the errors.

¹⁰ For the case of FF plus Comptonization distortion, the unperturbed CMB spectrum contribution was obviously already included in η .

spectrum being about one order of magnitude larger than the one for models with a monopole signal about 2 or 3 times smaller (compare Fig. 5 with Fig. 2). The richness of dipole profile morphology and of its sign changes can be, in principle, used as diagnostic for probing the underlying model.

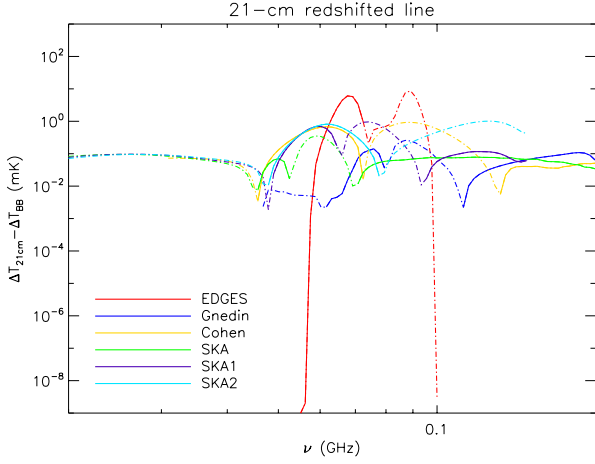


Fig. 5. Spectrum of dipole (in equivalent thermodynamic, or CMB, temperature) expressed as the difference between the one produced by the 21-cm redshifted line (summed in intensity with the CMB blackbody) for the monopole models as in Fig. 2 and the one corresponding to the blackbody at the current temperature T_0 . Thick solid lines (or three dots-dashes) correspond to positive (or negative) values. See also the legend and the text.

In Fig. 6 we display the dipole spectra derived for the radio extragalactic background signals with the same convention adopted before.

In this representation, the simple monopole power law dependence of the radio extragalactic background monopole is reflected into the power law dependence of the dipole spectrum, with a very similar spectral index. This can be simply understood expanding Eq. (17) to first order in Taylor series for $\eta \gg 1$ and considering that, at the frequencies of interest here, the CMB photon occupation number can be approximated as $1/x$. We will discuss this aspect in the next section, in combination with FF plus Comptonization distortions.

We report in Fig. 6 the dipole spectra corresponding to the extragalactic background emission by Seiffert et al. (2011) and to the extragalactic source global radio background by Gervasi et al. (2008a), while, for simplicity, we only show the dipole spectra corresponding to the minimum and maximum (identified here with the labels Low and High) of the residual monopole signals in Fig. 3 (namely, from Eq. (14) for $A = 4.7$ and 0.151 mK) since they scale linearly with A .

5. Signal combination results

We present the dipole spectra for several combinations of signals.

The comparison between Figs. 4, 5 and 6 clearly indicates that, at radio frequencies, the dipole spectrum from the global extragalactic background (see the two top lines in Fig. 6) overwhelms the ones from other signals. Therefore, when considering signal combinations, we apply source subtractions down to faint fluxes. Being mainly interested in the dipole spectrum at radio frequencies, we focus on the case of Comptonization distortion with $u = 2 \times 10^{-6}$, representative of imprints expected in

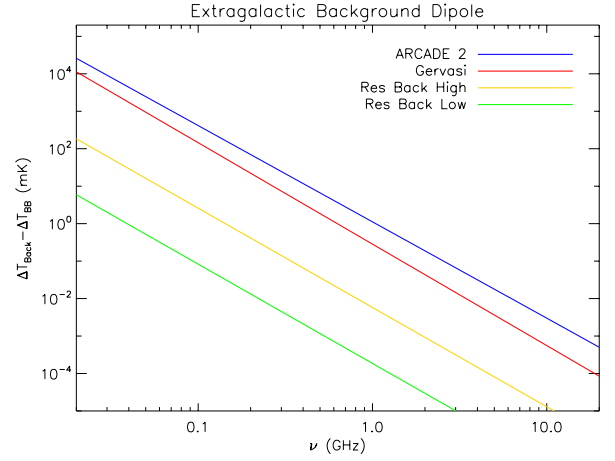


Fig. 6. Spectrum of dipole (in equivalent thermodynamic, or CMB, temperature) expressed as the difference between that produced by the radio extragalactic background signals (summed in intensity with the CMB blackbody) for the monopole models as in Fig. 3 and that corresponding to the blackbody at the current temperature T_0 . See also the legend and the text.

astrophysical models. Indeed, for lower values of u , the transition from the FF diffuse emission to the Comptonization distortion regime translates to higher frequencies (see Fig. 4).

Fig. 7 shows our main results. The panels in the two columns refer the low and high residual extragalactic background signals (see Fig. 6). The label in each panel stands for the adopted 21-cm redshifted line model. Different colors identify different signal combinations. In all panels, the two discussed FF models, with very different amplitudes, are exploited.

The blue (yellow) lines indicate the higher (lower) FF diffuse emission plus Comptonization distortions, the 21-cm redshifted line and the residual extragalactic background, as derived from Eq. (16) summing in η the corresponding photon occupation numbers, while in the green (violet) lines the residual extragalactic background is not included. For a lower residual background, the dipole from the four signals combination is almost identical to the one derived neglecting the residual background (the blue lines are masked by the green lines in the left panels). This does not hold in the case of a higher residual background (and the yellow and violet lines are distinguishable in all the panels).

According to the model, the contribution from the 21-cm redshifted line appears as a modulation of the dipole spectrum from signal combinations (see blue and yellow lines), affecting its approximate (see discussion below) power law dependence at frequencies between about 60 MHz and 200 MHz. As expected, this feature is more evident for models with larger and steeper monopole signals, and it is remarkable for the EDGE profile. Assuming to have subtracted the contribution of the residual background, the 21-cm redshifted line modulation is more or less evident over the FF emission dipole spectrum depending on their relative amplitudes (compare green and violet lines). For a lower FF emission, also the dipole sign inversions associated to these modulations is appreciable, according to the model, in the combination of all signals and obviously better when the residual background is subtracted (see yellow and violet lines).

Assuming that also the contribution of the FF diffuse emission could be accurately subtracted, the 21-cm redshifted line dipole spectrum emerges. This is shown by the red and light blue

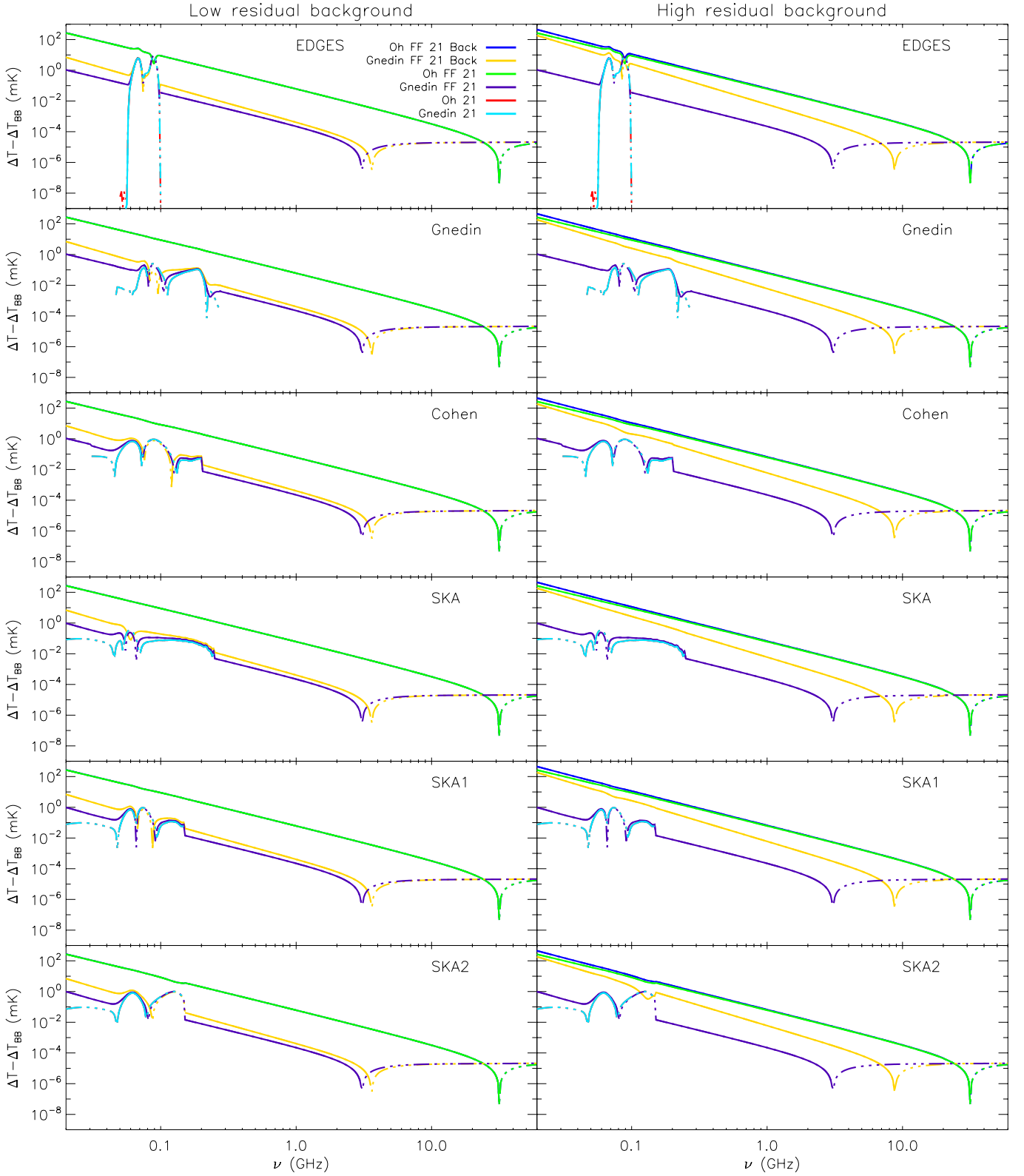


Fig. 7. Spectrum of dipole (in equivalent thermodynamic, or CMB, temperature) expressed as the difference between that produced by the combinations of signals and that corresponding to the blackbody at the current temperature T_0 . Thick solid lines (or thin three dots-dashes) correspond to positive (or negative) values. See also the legend and the text.

lines¹¹ in Fig. 7, but, remarkably, the main features displayed by

¹¹ Since they are ideally identical, the red line is masked by the light blue one, the little differences appearing at extremely low values in the

case of EDGES being due only to numerical accuracy, since the two curves are derived by subtraction starting from the two different global dipole predictions.

the light blue lines are visible also in the violet lines and, for a lower residual extragalactic background, even in the yellow lines, leaving room for the extraction, although challenging, of the 21-cm redshifted line dipole spectrum contribution embedded in the other background dipoles.

On a wide radio frequency range, far from the 60–200 MHz interval, the slopes of the dipole spectra of the four signals combination (blue and yellow lines) are between the steeper one, corresponding to the residual extragalactic background, and the flatter one, corresponding to the FF diffuse emission, according to the different amplitudes of the two types of signals. Eq. (17) allows us to derive a suitable approximation for the dipole spectrum from the combination of FF diffuse emission plus Comptonization distortion and extragalactic background in the Rayleigh-Jeans region, where $\eta \gg 1$. According to Eqs. (5), (9), (10) and Eqs. (12)–(14), let us assume

$$\eta = \frac{1 - 3u}{x} + bx^{-(\alpha+1)} + fx^{-(\xi+1)}, \quad (18)$$

where u quantifies the amplitude of Comptonization distortion, b and α (or f and ξ) characterize the extragalactic background (or the FF diffuse emission); here $\alpha \simeq 2.57 - 2.707$ and $\xi = 2 + \zeta \simeq 2.15$. In the limit $\eta \gg 1$, $(1 + \eta) \ln^2(1 + 1/\eta) \simeq 1/\eta$. Eq. (18) implies

$$\frac{d \ln \eta}{d \ln x} = -(1 + G), \quad (19)$$

with

$$G = \frac{b\alpha x^{-\alpha} + f\xi x^{-\xi}}{(1 - 3u) + bx^{-\alpha} + fx^{-\xi}}. \quad (20)$$

Finally, considering that for a blackbody spectrum at temperature T_0 we have simply $\Delta T_{\text{th}}^{\text{BB}} = \beta T_0$, after some algebra, Eq. (17) gives

$$\Delta T_{\text{th}} - \Delta T_{\text{th}}^{\text{BB}} \simeq F_1 + F_2 + F_3 + F_4, \quad (21)$$

where

$$F_1 = \beta T_0 b x^{-\alpha} (1 + G) \quad (22)$$

$$F_2 = \beta T_0 f x^{-\xi} (1 + G) \quad (23)$$

$$F_3 = \beta T_0 (1 - 3u) G \quad (24)$$

$$F_4 = -3\beta T_0 u. \quad (25)$$

The terms F_1 and F_3 with $u = 0$ and $f = 0$ give the result considering only the extragalactic background:

$$\Delta T_{\text{th}}^{\text{Back}} - \Delta T_{\text{th}}^{\text{BB}} \simeq \beta T_0 b x^{-\alpha} (1 + \alpha) = \beta T_{\text{ant}}^{\text{Back}} (1 + \alpha), \quad (26)$$

since $b x^{-\alpha} = T_{\text{ant}}^{\text{Back}} / T_0$.

Analogously, considering also Eq. (8) (obviously with $T_r = T_0$), the terms F_2 and F_3 with $u = 0$ and $b = 0$ give the result considering only the FF diffuse emission:

$$\Delta T_{\text{th}}^{\text{FF}} - \Delta T_{\text{th}}^{\text{BB}} \simeq \beta T_0 f x^{-\xi} (1 + \xi) \simeq \beta \Delta T_{\text{exc}}^{\text{FF}} (1 + \xi), \quad (27)$$

since $f x^{-\xi} = y_B / x^2$.

The term F_4 provides the result considering only the Comptonization distortion.

At low frequencies, Figs. (4) and (6) reflect the above relations. The same holds for Fig. (7), except for the further contribution, relevant in the ~ 60 –200 MHz range, from the 21-cm redshifted line. As discussed above, the different weights of the processes and the coupling between them, see Eqs. (20)–(25), determine the overall dipole spectrum. The condition $F_2 + F_3 + F_4 = 0$ with $b = 0$ and the approximation $1 - 3u \simeq 1$ gives the solution

$$x_0^{\text{FF,C}} = \left(\frac{h\nu_0^{\text{FF,C}}}{kT_0} \right) \simeq \left[\frac{A_{\text{FF}}}{3u} (1 + \xi) \left(\frac{h \cdot 1\text{GHz}}{kT_0} \right)^{\xi-1} \right]^{1/\xi} \quad (28)$$

for the frequency of the sign change corresponding to the transition from the FF to the Comptonization regime (see Fig. 4). Obviously, because of the assumption $\eta \gg 1$ and the simple power law approximation for y_B , the accuracy of Eq. (28) degrades at increasing frequency. The comparison with Fig. 4, based on Eq. (16) without further approximations, shows that it works well (or overestimates $\nu_0^{\text{FF,C}}$) for the lower (or for the higher) FF diffuse emission, compared to the amplitude of Comptonization distortion.

Remarkably, Fig. 7 shows that, for the case of a lower FF diffuse emission, the frequency of sign change (at around 3 GHz in Fig. 4) when the Comptonization distortion begins to dominate, moves to higher frequencies because of the contribution from residual extragalactic background (compare violet and yellow lines). This effect is obviously more evident for a higher residual extragalactic background (compare left and right panels). An upper limit to this frequency of sign change can be derived from the condition $F_1 + F_3 + F_4 = 0$ with $f = 0$ and the approximation $1 - 3u \simeq 1$. This gives

$$\left(\frac{\nu_0^{\text{Back,C}}}{\text{GHz}} \right) = \left(\frac{kT_0}{h} x_0^{\text{Back,C}} \right) \lesssim \left[\frac{A(1 + \alpha)}{3T_0 u} \right]^{1/\alpha}. \quad (29)$$

For a much higher FF diffuse emission this frequency shift becomes almost negligible.

With a wide frequency coverage, it would be possible to appreciate the different shapes of the various dipole signals. Microwave surveys are particularly important for the assessment of the Comptonization distortion contribution to the dipole spectrum, thus improving the modeling of the FF term at lower frequencies. A certain frequency shift to higher values of the transition of the Comptonization distortion regime can be expected also for lower values of u (see Fig. 4) because of the residual background contribution. Toward microwave frequencies, extragalactic sources with an almost flat spectrum, not so well described by the adopted number counts, become of increasing relevance. They can be extracted directly analyzing CMB maps from next space mission generation or using deeper multifrequency ground-based surveys (see, e.g., De Zotti et al. (2018) and references therein for a deeper discussion).

6. Discussion and conclusion

The best way to study the dipole spectrum of cosmic diffuse emissions should be based on the analysis of nearly all-sky or very wide coverage surveys. On the other hand, investigations at microwave to sub-millimetre frequencies take advantage from avoiding sky regions mostly affected by foreground signals, in spite of the partial reduction of the observed area.

Surveys at radio frequencies are performed through "classical" mapping from single telescopes or with interferometric

techniques involving a large number of telescopes, aimed, in particular, at improving resolution and sensitivity at small scales.

According to the implemented configuration (i.e. the adopted baselines), interferometers are intrinsically sensitive to sky signal variations up to certain spatial scales (typically, of several degrees), thus producing a wide area map collecting different patches, essentially independently, and preventing the analysis of sky geometrical properties at angular scales larger than the patch. The map could be, in principle, reconstructed with suitable array designs and observational approaches, such as a compact configuration implementing short baselines and a high uv-space filling factor, mosaicing techniques and, for the largest areas, methods such as on-the-fly-mapping. Furthermore, it is possible to recalibrate different sets of interferometric maps over wide area surveys taken with "classical" (single dish) approaches, such to recover the information at large scales but keeping interferometric sensitivity and resolution at small scales.

If these approaches, useful for a broad set of SKA scientific projects, will work successfully, the analysis of diffuse cosmic dipoles at radio frequencies could be pursued with methods analogous to those suitable for CMB recent surveys and future missions (Burigana et al. 2018). The analysis of these aspects and of the applications of those methods, readapted to the radio domain, as well as the investigation of specific techniques to deal with independent patches from interferometric observations will be object of a future study.

Differently, the dipole pattern amplitude reconstruction could be carried out not necessarily requiring a coherent mapping up to the largest angular scales. Indeed, along a meridian in a reference frame with z-axis parallel to the dipole direction, the signal variation at colatitude θ from a dipole pattern with ΔT – see Eq. (16) – within a limited sky area of linear size $\Delta\theta$, has an amplitude $|\Delta T_{\Delta\theta}| \simeq \Delta T \cdot (\Delta\theta/90^\circ) \sin \theta$, with $\sin \theta$ not far from unit at angles large enough from the poles.

At $\nu \sim (50 - 100)$ MHz, for the FF and 21-cm signatures we find that the relevant signals (once subtracted the standard CMB blackbody spectrum dipole) have amplitudes $\Delta T_{\text{th}} - \Delta T_{\text{th}}^{\text{BB}} \sim 0.1 - 50$ mK depending on the model. Similar values hold also for the radio extragalactic background when considering deepest detection thresholds. Values of about 2 (or 4) orders of magnitude larger are achieved for shallower detection limits (or for the radio extragalactic background best fit signal). Thus, for a patch of size $\Delta\theta \sim 3^\circ$, sensitivities to the diffuse signal of \sim several tens of mK (or in a range from \sim a few μK to \sim mK) could allow to identify the extragalactic background (or the reionization imprints in the diffuse radio dipole). Subtracting sources applying a broad set of detection thresholds would also help to clarify how much the radio extragalactic background could be ascribed to extragalactic sources or being of intrinsic cosmological/diffuse origin, contributing to unravel the question about the level and origin, still controversial (see, e.g., Subrahmanyan & Cowsik (2013); Hills et al. (2018); Sharma (2018)), of the radio extragalactic background. Obviously, collecting many patches would improve the statistical information.

In general, an ultra-accurate subtraction of the Galactic foreground emission is the most critical issue for analyzing fine cosmological signals. Differently from Galactic foreground, all the signal variations in the patches from cosmic diffuse dipoles should be described by a well defined pattern related to the observer motion, and this would improve their joint analysis.

The study of dipole spectrum, linking monopole and anisotropy analyses, relies on the quality of interfrequency and relative data calibration, in principle by-passing the need for precise absolute calibration, that is a delicate task in cosmological

surveys and, in particular, in the combined analysis of data from different experiments and of maps from radio interferometric facilities. Therefore, it could also represent a way to complement and cross-check investigations on cosmological reionization, based on the study of the global signal and of the fluctuations projected into the sphere, or in redshift shells performed with angular power spectrum or power spectrum analyses and higher order estimators.

Acknowledgements. It is a pleasure to thank Gianni Bernardi, Gianfranco de Zotti and Isabella Prandoni for useful discussions. We gratefully acknowledge financial support from the INAF PRIN SKA/CTA project FORMation and Evolution of Cosmic Structures (FORECaST) with Future Radio Surveys, from ASI/INAF agreement n. 2014-024-R.1 for the *Planck* LFI Activity of Phase E2 and from the ASI/Physics Department of the University of Roma–Tor Vergata agreement n. 2016-24-H.0 for study activities of the Italian cosmology community.

References

- Balashev, S. A., Kholupenko, E. E., Chluba, J., Ivanchik, A. V., & Varshalovich, D. A. 2015, *ApJ*, 810, 131
- Barkana, R. 2018, *Nature*, 555, 71
- Bernardi, G., Zwart, J. T. L., Price, D., et al. 2016, *MNRAS*, 461, 2847
- Bowman, J. D., Rogers, A. E. E., Monsalve, R. A., Mozdzen, T. J., & Mahesh, N. 2018, *Nature*, 555, 67
- Burigana, C., Carvalho, C. S., Trombetti, T., et al. 2018, *J. Cosmology Astropart. Phys.*, 4, 021
- Burigana, C., de Zotti, G., & Danese, L. 1995, *A&A*, 303, 323
- Burigana, C., Popa, L. A., Salvaterra, R., et al. 2008, *MNRAS*, 385, 404
- Burns, J. O., Lazio, J., Bale, S., et al. 2012, *Advances in Space Research*, 49, 433
- Cohen, A., Fialkov, A., Barkana, R., & Lotem, M. 2017, *MNRAS*, 472, 1915
- Danese, L. & de Zotti, G. 1981, *A&A*, 94, L33
- De Zotti, G., González-Nuevo, J., López-Cañiego, M., et al. 2018, *J. Cosmology Astropart. Phys.*, 4, 020
- De Zotti, G., Negrello, M., Castex, G., Lapi, A., & Bonato, M. 2016, *J. Cosmology Astropart. Phys.*, 3, 047
- Deshpande, A. A. 2018, *ApJ*, 866, L7
- Dowell, J. & Taylor, G. B. 2018, *ApJ*, 858, L9
- Ewall-Wice, A., Chang, T.-C., Lazio, J., et al. 2018, *ApJ*, 868, 63
- Feng, C. & Holder, G. 2018, *ApJ*, 858, L17
- Fixsen, D. J. 2009, *ApJ*, 707, 916
- Fixsen, D. J., Cheng, E. S., Gales, J. M., et al. 1996, *ApJ*, 473, 576
- Forman, M. A. 1970, *Planet. Space Sci.*, 18, 25
- Furlanetto, S. R., Oh, S. P., & Briggs, F. H. 2006, *Phys. Rep.*, 433, 181
- Gao, L. & Theuns, T. 2007, *Science*, 317, 1527
- Gervasi, M., Tartari, A., Zannoni, M., Boella, G., & Sironi, G. 2008a, *ApJ*, 682, 223
- Gervasi, M., Zannoni, M., Tartari, A., Boella, G., & Sironi, G. 2008b, *ApJ*, 688, 24
- Gnedin, N. Y. 2000, *ApJ*, 542, 535
- Hills, R., Kulkarni, G., Meerburg, P. D., & Puchwein, E. 2018, *Nature*, 564, E32
- Mirabel, I. F. 2019, *arXiv e-prints [arXiv:1902.00511]*
- Muñoz, J. B. & Loeb, A. 2018, *ArXiv e-prints*, 1802.10094
- Oh, S. P. 1999, *ApJ*, 527, 16
- Planck Collaboration. 2016a, *A&A*, 594, A1
- Planck Collaboration. 2016b, *A&A*, 594, A5
- Planck Collaboration. 2016c, *A&A*, 594, A8
- Planck Collaboration, Aghanim, N., Akrami, Y., et al. 2018a, *arXiv e-prints [arXiv:1807.06209]*
- Planck Collaboration, Aghanim, N., Akrami, Y., et al. 2018b, *arXiv e-prints [arXiv:1807.06207]*
- Planck Collaboration, Akrami, Y., Argüeso, F., et al. 2018c, *arXiv e-prints [arXiv:1807.06206]*
- Ponente, P. P., Diego, J. M., Sheth, R. K., et al. 2011, *MNRAS*, 410, 2353
- Prandoni, I., Guglielmino, G., Morganti, R., et al. 2018, *MNRAS*, 481, 4548
- Prandoni, I. & Seymour, N. 2015, *Advancing Astrophysics with the Square Kilometre Array (ASKA14)*, 67
- Pritchard, P. R. & Loeb, A. 2010, *Phys. Rev. D*, 82, 023006
- Retana-Montenegro, E., Röttgering, H. J. A., Shimwell, T. W., et al. 2018, *A&A*, 620, A74
- Salvaterra, R. & Burigana, C. 2002, *MNRAS*, 336, 592
- Schneider, R., Salvaterra, R., Choudhury, T. R., et al. 2008, *MNRAS*, 384, 1525
- Seiffert, M., Fixsen, D. J., Kogut, A., et al. 2011, *ApJ*, 734, 6
- Sharma, P. 2018, *MNRAS*, 481, L6
- Singal, J., Fixsen, D. J., Kogut, A., et al. 2011, *ApJ*, 730, 138

- Slosar, A. 2017, *Physical Review Letters*, 118, 151301
- Subrahmanyan, R. & Cowsik, R. 2013, *ApJ*, 776, 42
- Subrahmanyan, R., Shankar, U. N., Pritchard, J., & Vedantham, H. K. 2015, *Advancing Astrophysics with the Square Kilometre Array (AASKA14)*, 14
- Trombetti, T. & Burigana, C. 2014, *MNRAS*, 437, 2507
- Vernstrom, T., Scott, D., Wall, J. V., et al. 2014, *MNRAS*, 440, 2791
- Vernstrom, T., Scott, D., Wall, J. V., et al. 2016, *MNRAS*, 462, 2934
- Viel, M., Lesgourgues, J., Haehnelt, M. G., Matarrese, S., & Riotto, A. 2005, *Phys. Rev. D*, 71, 063534
- Zel'dovich, Y. B., Illarionov, A. F., & Sunyaev, R. A. 1972, *Soviet Journal of Experimental and Theoretical Physics*, 35, 643

Appendix A: Estimate of ν_B

We will discuss here the frequency range validity of the FF distortion approximation in terms of the parameter y_B (see Eqs. (2), (4) and (7)). It holds at dimensionless frequencies $x_B \ll x \ll 1$ (see Burigana et al. (1995) and references therein), where x_B is such that $y_{abs,B}(x_B) = 1$, being

$$y_{abs,B}(x, \phi(z), z) = \int_1^{1+z} \frac{t_{exp} d(1+z')}{t_{abs,B}(1+z')}, \quad (\text{A.1})$$

where $t_{abs,B}$ is the bremsstrahlung absorption time

$$\frac{1}{t_{abs,B}} = K_B(z) \frac{g(x, \phi)}{(x/\phi)^3} e^{-x/\phi} (e^{x/\phi} - 1). \quad (\text{A.2})$$

The expansion time, including the contributions of the different types of energy densities in a Friedmann-Lemaître-Robertson-Walker model, can be expressed by

$$t_{exp} = \frac{a}{\dot{a}} = \frac{1}{H(z)} = \frac{1}{\left[H_0 \Omega_{rel}^{1/2} (1+z)^2 \right] \left[1 + \frac{\Omega_m/\Omega_{rel}}{1+z} \left(1 + \frac{\Omega_K/\Omega_m}{1+z} + \frac{\Omega_\Lambda/\Omega_m}{(1+z)^3} \right) \right]^{1/2}} \quad (\text{A.3})$$

where Ω_{rel} , Ω_K and Ω_Λ are the relativistic particle (typically radiation plus relativistic neutrinos) density parameter, the curvature density parameter and the cosmological constant – or dark energy, or vacuum energy – density parameter.

At $x \ll 1$, in Eq. (A.2) $[g(x, \phi)/(x/\phi)^3] e^{-x/\phi} (e^{x/\phi} - 1) \simeq g(x, \phi) \phi^2 / x^2$. Thus, the condition $y_{abs,B}(x_B) = 1$ becomes

$$\begin{aligned} x_B^2 &\simeq \int_1^{1+z} \frac{t_{exp}}{(1+z')} K_B(z') g(x_B, \phi) \phi^2 d(1+z') \\ &\simeq 1.6 \cdot 10^{-7} (T_0/2.7\text{K})^{-7/2} \\ &\cdot \int_1^{1+z} \frac{\Omega_b^2 h_{50}^3 \chi_e^2 \phi^{-3/2} g(x_B, \phi) d(1+z')}{\left\{ \Omega_{rel}(1+z') \left[1 + \frac{\Omega_m/\Omega_{rel}}{1+z'} \left(1 + \frac{\Omega_K/\Omega_m}{1+z'} + \frac{\Omega_\Lambda/\Omega_m}{(1+z')^3} \right) \right] \right\}^{1/2}}. \end{aligned} \quad (\text{A.4})$$

For simplicity, we consider first in the integral only the terms at denominator with explicit dependence on z' ; we will discuss later the impact of the other evolving terms. In reionization context $z' < \text{few tens}$ and then $\Omega_{rel}(1+z') \ll 1$, thus neglecting the curvature term, significantly constrained by recent data and impacting the result less than a few per cent, the integral in the above equation becomes $\sim \Omega_m^{-1/2} \int_1^{1+z} (1+z')^{3/2} d(1+z') / [(1+z')^3 + \Omega_\Lambda/\Omega_m]^{1/2} \lesssim \Omega_m^{-1/2} z$. An upper limit to x_B is then

$$x_B \lesssim 4 \cdot 10^{-4} (T_0/2.7\text{K})^{-7/4} \Omega_b \Omega_m^{-1/4} h_{50}^{3/2} \chi_e \phi^{-3/4} g(x_B, \phi)^{1/2} z^{1/2}. \quad (\text{A.5})$$

For cosmological parameters compatible with current data (Planck Collaboration et al. 2018a), Eq. (A.5) implies $x_B \lesssim 4 \cdot 10^{-5} \chi_e \phi^{-3/4} g(x_B, \phi)^{1/2} z^{1/2}$, that, in terms of observational frequency, corresponds to $\nu_B / [\chi_e \phi^{-3/4} g(x_B, \phi)^{1/2}] \lesssim 10 \text{ MHz}$ (or $\lesssim 3.2 \text{ MHz}$) for $z \simeq 20$ (or 2). Being $g(x_B, \phi) \approx 1$ and $\chi_e \lesssim 1$, possible relevant modifications to this estimate can come only from the evolution of ϕ . The adopted value of Ω_b corresponds to an homogeneous medium, and this should be multiplied by $(1 + \sigma^2(z))^{1/2}$ because

of inhomogeneities (see the discussion in Sect. 2.1). This factor could significantly increase ν_B only at $z \lesssim \text{few units}$ and up to, at most, one order of magnitude. This is largely compensated by the former effect due to electron temperature evolution (the term $\phi^{-3/4}$) that for typical reionization thermal histories with $T_e \sim 10^4 \text{ K}$ implies a decreasing of ν_B by more than two orders of magnitude at $z \lesssim 6$.

Thus, at observational frequencies $\gtrsim 10 \text{ MHz}$, relevant for radio observations, the approximation of the FF distortion in terms of y_B is robust for the large majority of models.